Modelling of 3D Temperature Behavior of Prismatic Lithium-Ion Cell With Focus on Experimental Validation Under Battery Electric Vehicle Conditions

Jan Kleiner*, Lidiya Komsiyska, Gordon Elger and Christian Endisch

Technische Hochschule Ingolstadt, Institute of Innovative Mobility, Ingolstadt, Germany

*Corresponding Author: jan.kleiner@thi.de, +49(0)841 9348 – 6419

Abstract

The electrification of vehicles focuses on battery electric vehicle (BEV) concepts with lithium-ion battery systems where temperature has a great impact on performance, safety and lifetime. Modelling the thermal behavior of lithium-ion batteries enables researchers to investigate the temperature distribution under different cooling conditions in detail. Model validation with experimental tests is necessary to ensure meaningful simulation models. Therefore, experiments have to be performed under defined conditions with a distinct understanding of influences, so that they can be used for validation. In this paper, a 3D electro-thermal battery model is developed and parametrized. An experimental setup with defined external influences is designed which takes the conditions of a lithium-ion cell in a BEV use case into account. Experimental tests with prismatic cells are performed for different charging profiles and finally, the thermal behavior of the model is validated under experimental conditions of BEV scenario with a spatial resolution of temperature.

1 Introduction

Electric vehicles (EVs) are seen as a solution to reduce car emissions for automotive manufactures to fulfill the continuously rising environmental regulations [1,2]. The ongoing electrification of vehicles is focused on battery electric vehicles (BEVs) with lithium-ion based battery systems due to their high specific energy, low self-discharge and long cycle-life [2,3]. Various battery design concepts are used in BEVs using pouch, cylindrical, and prismatic lithium-ion cells with or without module architecture. Depending on the used cell type, different cooling concepts are utilized that are based on air, liquid and other different approaches [1]. For lithium-ion batteries, temperature has a significant influence on the battery performance, aging and safety [3]. Therefore, cooling conditions and resulting thermal cell behavior are important to investigate.

To characterize the thermal behavior of battery cells in automotive applications, researchers focus on modelling the thermal phenomena [4-7]. They develop different electro-(chemical)-thermal coupled simulations based on the general energy balance for lithium-ion based systems [8]. Usually the model behavior is validated with experimental results. However, the boundary conditions of the experiments are often not well defined and differ from the boundary conditions within the model. This influences significantly the simulated thermal behavior, complicates the model validation, and introduces additional uncertainties.

Building a well-defined experimental setup is challenging because the main goals are often contradicting. The aim is to design an experimental setup that guarantees reproducible boundary conditions for simulation and represents a realistic use case scenario for later investigations. Erhard developed an experimental setup especially for a pouch-cell in a wind tunnel to obtain knowledge of the cooling conditions such as air velocity for meaningful thermal validation [5].

Samad et al. use similar conditions in development and validation of their battery model of a pouch cell with air-cooling [6].

Another investigated concept in literature is liquid cooling for prismatic cells in module architecture [6,7]. Damay et al. introduced a lumped thermal model coupled with an electrical model for representation of the main thermal phenomena [6]. The authors account for experimental influences and thermal boundary conditions. However, a lumped thermal model has low significance for a spatially-resolved validation of simulation results and conclusions about the 3D thermal behavior inside the cell. Lundgren et al. suggested a detailed 3D electrochemical-thermal model with experimental validation [7]. However, they did not consider experimental influences such as heat flux between battery tester and cell or mechanical cell environment.

Commonly, prismatic cells are stacked in modules and compressed for better performance. In this concept, the temperature difference between cells inside a single module is expected to be small and therefore negligible. The only heat sink is given by the cooling system at the bottom of the cell [6]. Cooling is energy consuming and does not run at all times, as long as the battery temperature is in the desired range between 25 – 40°C [9]. Thermal BEV conditions in this work are assumed to be mostly adiabatic for a single prismatic cell due to module architecture. Only at the bottom, a constant cooling temperature of 30°C is defined.

The goal of this work is to combine a detailed 3D electro-thermal model with well-known boundary conditions from defined experimental investigations that represents the use of battery cells in electric vehicles. The approach comprises electro-chemical heat generation and heat conduction in lithium-ion batteries. With precise parametrization and spatial validation, a meaningful thermal model is designed to analyze the temperature inside a prismatic battery cell.

ISBN 978-1-7281-2078-2

2 Modelling

2.1 Multi-scale multi-dimensional approach

Modelling lithium-ion battery behavior is challenging due to the non linear physico-chemical processes occurring on different length scales. In the current contribution, a multi-scale multi-dimensional [MSMD] approach was adopted, which is described in the literature [10]. With MSMD approach, the different phenomena are solved on multiple domains with hierarchical structure by sub-models with different length scales [10]. The approach is flexible in the choice of sub-models as long as they follow the predefined exchange of information between domains [10]. Implemented in ANSYS Fluent CFD as *MSMD battery model*, the main equations calculated on the mesh of 3D thermal geometry are [11]

$$\frac{\partial \rho \cdot C_p \cdot T}{\partial t} - \nabla[\, k \cdot \nabla T\,] = \dot{q}_{ECh} + \dot{q}_{Ohm} \qquad (1)$$

$$\nabla[\, \sigma_+ \cdot \nabla \varphi_+\,] = -j_{ECh} \qquad (2)$$

$$\nabla[\, \sigma_- \cdot \nabla \varphi_-\,] = j_{ECh} \qquad (3)$$

whereat *(1)* is the spatial energy balance with the first term as the internal energy including density ρ, specific heat capacity C_p , and temperature T. The second term implies heat conduction with heat transfer coefficient k and the right hand site of *(1)* shows $\dot{q}_{Ohm}$ as the generated heat by ohmic resistances and $\dot{q}_{ECh}$ as reaction heat due to electrochemical reactions. Equation *(2)* and *(3)* are potential equations for the calculation of two electrical fields where φ is the phase potential on positive/negative electrode, j_{ECh} is the volumetric current transfer density, and σ the effective electric conductivity for materials of positive and negative electrode [11]. With this approach, the cell's thermal behavior is modelled, using a 3D thermal model for heat conduction and an electrical sub-model for heat generation.

2.2 Thermal model

In this paper a prismatic lithium-ion battery cell by SANYO/Panasonic with NMC chemistry is used. The nominal capacity is 25Ah. For the development of detailed 3D CAD geometry a post mortem and computer tomographic analysis are performed. The resulting simplified CAD geometry is shown in figure 1 and the corresponding materials with physical properties are listed in table 1. The jelly roll is modelled as a solid body, while the real jelly roll has a layered structure of positive/negative electrode with active materials, electrolyte, and separator. The homogenized modelled jelly roll still contains anisotropic thermal conductivity for high conductive in-plane direction and low conductive through-plane direction [7,12]. Values for conductivity are obtained from producer's data sheet to 33 / 0.7 [$Wm^{-1}\,K^{-1}$], which fit well to previously reported values of 30.8 / 0.95 [$Wm^{-1}\,K^{-1}$] and 37 / 0.5 [$Wm^{-1}\,K^{-1}$] [7,12]. The heat generation inside the jelly roll is modelled as volumetric heat source and calculated in the electrical sub-model.

The material *Copper* in table 1 is used as negative terminal and current collector and *Aluminum* for positive terminal and current collector. Furthermore, *Aluminum* with reduced thermal conductivity is used for the casing due to lower purity. Electrical insulating sheets e.g. between case and jelly roll are modelled as *thin walls* without a geometrical body to mesh. Nevertheless, trough-plane heat conduction is considered based on given material thickness and thermal conductivity [11]. The same modelling approach is applied for thermal connection to the cooling plate.

The symmetric 3D cell model is solved as half reduced model with a mesh containing 69k elements. The maximal adaptive time step is set to 5s with logarithmic rise starting at 0.1s at every current change in the used profile.

Table 1: Physical and thermal properties of the materials used for modelling of 3D CAD geometry of prismatic cell.

Material	ρ [kg m^{-3}]	C_p [J $kg^{-1}\,K^{-1}$]	λ [$Wm^{-1}\,K^{-1}$]
Aluminum[a]	2700	900	238
Copper[a]	8700	385	400
Insulation[b]	1470	1190	0.18
Thermal pad[c]	2740	903	2.22
Jelly roll[a]	2043	1371	in-plane 33[d] through-plane 0.7[d]

[a] [12], [b] [7], [c] data sheet, [d] data sheet

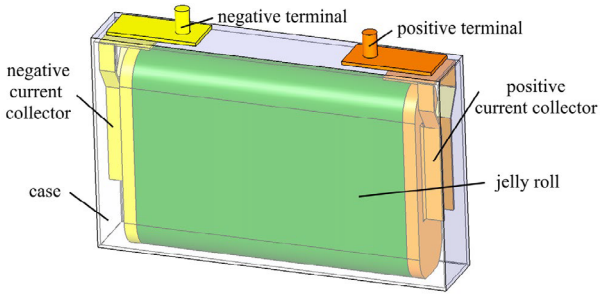

Figure 1: 3D CAD geometry of battery cell model with jelly roll, current collectors, terminals, and case

Correct model performance in validation is guaranteed by consideration of experimental conditions in simulation. The following boundary conditions are defined additionally to reproduce experimental conditions (figure 2):

- Cell bracing/measurement plates modelled as solid bodies containing mass and thermal properties
- Constant temperature boundary of 30°C on the cell bottom including thermal pad in between
- Transient heat flux profile at the terminals

ISBN 978-1-7281-2078-2

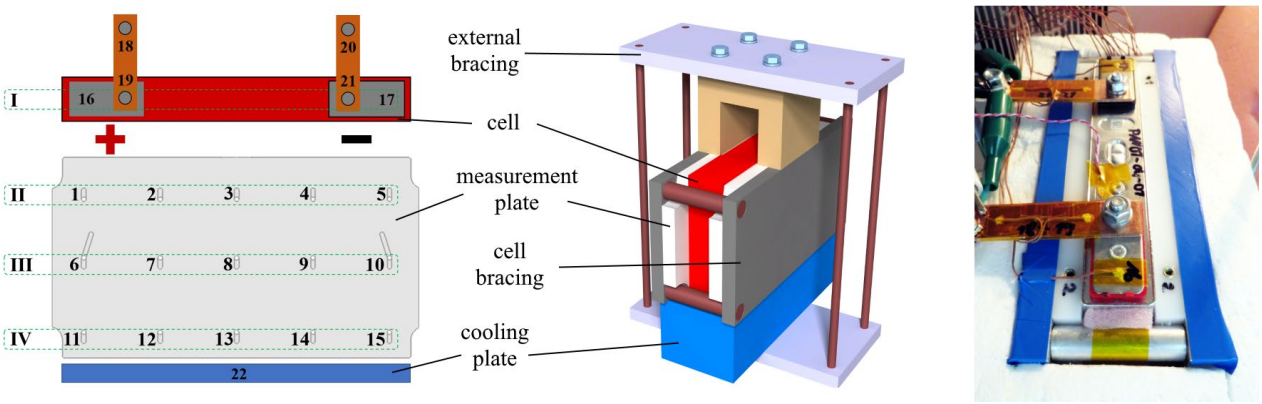

Figure 2: Experimental setup: Schematics and nomenclature of temperature sensors (left), concept of experimental setup (middle), and top view photograph of the cell with insulation (right).

The transient heat flux profile takes into account the transferred heat between the cell and the battery tester through the wiring. In each experiment, temperature differences on the busbars are measured and the corresponding heat flux is calculated. This profile is used as boundary conditions at the terminals in the simulation. Constant temperature boundary conditions reproduce the experimental conditions of the cooling plate with a constant temperature of 30°C. The thermal pad in between guarantees planar thermal contact but generates a thermal resistance as well.

For later investigations of the temperature distribution, the boundary conditions are set on BEV conditions without particular influences of experimental setup. For model validation, these conditions, such as bracing and terminal heat flux, have to be considered mandatorily.

2.3 Electrical model

The sub-model for electrical behavior of the cell and corresponding heat generation is implemented as a user defined 1RC equivalent circuit model (ECM). The state-of-charge (SOC) and temperature-depended RC-parameters are fitted on experimental hybrid pulse power characteristic (HPPC) measurement data of the used prismatic cell. Based on this, the positive/negative potentials and SOC in a single element in the jelly roll domain are calculated for every time step. Subsequently, equation *(4)* is used for calculating the time-dependent heat generation in a lithium-ion system [8]:

$$\dot{q} = j \cdot [\, U_{OCV} - U \,] + j \cdot T \cdot \frac{dU_{OCV}}{dT} \qquad (4)$$

The battery voltage U is computed in ECM sub-model. With knowledge of the current density j from MSMD information exchange and batteries open circuit voltage U_{OCV} the irreversible heat generation in the first term of *(4)* is calculated. The second term shows the reversible heat due to entropy change calculated with current density j, temperature T, and the entropic heat coefficient dU_{OCV}/dT. This coefficient, which is depending on the battery chemistry and changing with SOC, is taken from the literature [13].

Heat generation in the current collectors is modelled as ohmic losses, represented in *(1)* as $\dot{q}_{Ohm}$. The heat is calculated with the information of the potential equations *(2)* and *(3)* based on electrical resistances from additional experiments. Normally, the contact resistances in this model are expected to be negligible. In case of the current collectors the resulting contact resistances of overall 70 electrically-contacted electrode sheets is considered.

The spatially-resolved heat generation is based on fitted RC-parameters. Most of these parameters, and thus the heat generation, change with SOC and temperature. Therefore, the HPPC tests in this work are performed for different temperatures and SOC levels. Depending on the used battery chemistry there can be additional other non linearites in cell's heat generation e.g. with further aging. Taking account of multi-dimensional dependencies, the RC-parameter data are organized as n-dimensional look-up tables with discrete points and interpolation mechanism. I.e. for consideration of aging, additional parameters can be integrated in the developed model structure. For this purpose, HPPC tests have to be performed with aged cells and subsequently aging-dependent parameters have to be fitted.

3 Experimental

To achieve the thermal conditions of BEV environment on single cell level, a measurement setup is designed and implemented, which is shown in figure 2. Thermal BEV conditions for a single prismatic cell are defined as adiabatic except the cooling system at the bottom. Similar to module conditions, the cell is clamped with aluminum bracing plates supplemented by polyoxymethylene (POM) measurement plates. To obtain spatially-resolved information about the temperature behavior 15 thermocouples type T class 1 with accuracy of ±0.5K are integrated in 3 rows and 5 columns inside the measurement plate (figure 2; left). Moreover, measurement on terminals, busbars and cooling plate are implemented. The thermocouples on the busbars are used to measure temperature differences and calculate the heat flux between cell and battery tester. All thermocouples are logged with PicoLog TC-08 data loggers and resulting values are summed up for evaluation with simulation in average values per row named I-IV.

ISBN 978-1-7281-2078-2

The desired boundary conditions of the BEV cooling system are achieved by a cooling plate with thermoelectric cooler regulation with constant temperature. A thermal pad as a gap filler is used to guarantee uniform thermal coupling between the cell and the cooling plate. Moreover, the assembly is placed in an additional compression unit in order to achieve defined and reproducible coupling between the cooling plate and the cell. The real setup (figure 2; right) is isolated with polystyrene foam to establish adiabatic conditions in all directions except for the cooling plate on the bottom side.

The start and working temperature for all validation tests is defined at 30°C realized by a temperature chamber Binder KB115 and the cooling plate. Prior to each experiment the cell is subjected to 4 hours tempering to ensure comparability in the starting conditions by removing thermal inhomogeneities.

The cell cycling is performed using a battery tester from Arbin (LBT 5V/60A). The used cycling profiles start with a discharge and are followed by an alternating discharge and charge profile with a 10s break in between. The current rate in the battery context is related to the nominal capacity of the used cell. The C-rate defined as current per nominal capacity guarantees comparability between different cells. A current of 75A for the 25Ah cell is equivalent to a C-rate of 3C. An exemplary profile for 3C is shown at the bottom of figure 3.

4 Results and Discussion

In order to examine the impact of the ambient conditions, several cell cycling test are performed using the same current profile under commonly used temperature of 25°C. Figure 3 shows the results for the adiabatic setup (*Adiabatic)*, with inactive temperature chamber (*TC off*), active temperature chamber (*TC on*) and the mimicked BEV conditions setup with cooling plate (*Plate*), operating at 25°C for comparison.

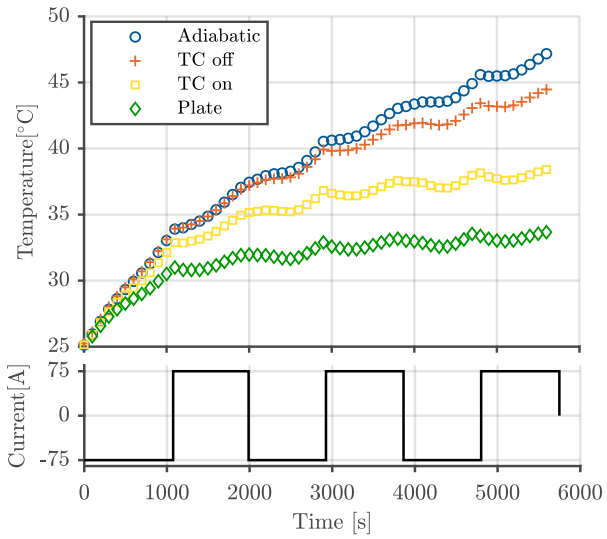

Figure 3: Top: Average cell temperature of 25Ah cell at 3C cycling with different ambient conditions each at 25°C. Bottom: Used 3C (75A) cycling profile.

With respect to the cycling profile at the bottom, the characteristic transient behavior of the cell in every cycle is apparent for all experiments. As expected, the temperature rises during the continuous cycling due to internal cell resistance, charge transfer, and diffusion resistances. However, the measured temperatures show significant dependence on the used ambient conditions.

Adiabatic conditions, often used in thermal runaway studies, show after 3 cycles the largest temperature increase of 22K. Since only the wiring to the battery tester functions as a (unwanted) heat sink, a heat flux to the battery tester is induced. The performed measurements show, that under the studied conditions this heat flux can increase up to 20% of the overall generated heat. This has a strong impact on the targeted adiabatic conditions. Based on this knowledge, the heat flux on terminals is measured additionally for all following experiments.

When the measurement is carried out in a non active temperature chamber (*TC off*), but still previously tempered, the cell reaches a temperature of 45°C (20K increase) at the end of the cycling. Whereas, when the chamber's recirculation is active (*TC on*), the average cell temperature reaches only 38°C. With deactivated temperature chamber, the cell is cooled by natural convection. However, the flow conditions are unknown, which further increases the modelling uncertainties. An active chamber cools the cell with forced convection but the flow conditions and the heat - transfer coefficient are unknown, too. Moreover, for the forced convection case, the cell temperature is also dependent on the position of the cell within the chamber.

Using the developed setup, mimicking BEV conditions including cooling plate, the lowest temperatures increase of 9K is observed. For these cooling conditions, an influence on the transient thermal behavior by the cell bracing construction is found. In contrast, no influence of the bracing onto the cooling plate on temperature behavior is detected.

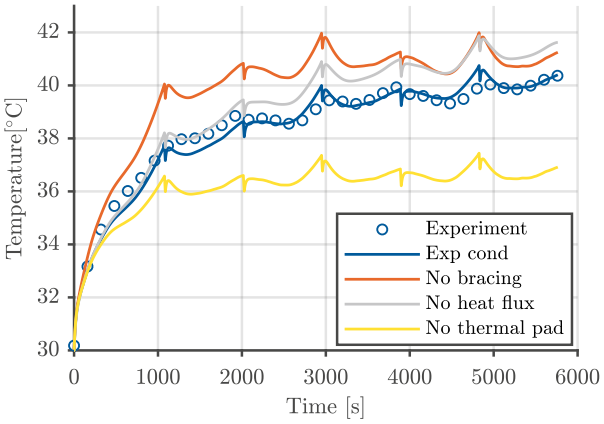

Figure 4: Average cell temperature of experiment, validated simulation model and simulation model without respectively modelling bracing, heat flux at terminals and thermal connection to cooling plate. Used setup is 25Ah cell at 3C cycling with BEV conditions at 30°C.

ISBN 978-1-7281-2078-2

To further examine the influence of the setup components on the modeling results, various simulations are performed, where different influences are deliberately neglected. In figure 4 the development of the average cell temperature during the experiment is compared to the deviating simulation results. Considering all boundary conditions of the designed setup for the simulation (*Exp cond*), the experimental results are in very good agreement with the simulation. It is apparent, that if the bracing components are neglected (*No bracing*) within the model the cell exhibits higher average temperature with a deviation of ~2K. The components of aluminum and POM have high thermal masses that influence the transient process of heating up. Not considering the heat consumption of the bracing leads to modeled cell temperatures higher than the real values at the beginning.

While the heat flux to the battery tester is not considered (*No heat flux*), the temperatures during the initial cycle still fit very well with the performed experiment. However, a significant temperature increase is visible for the consecutive cycling, giving rise to a mismatch >1K. If no thermal contact resistance to the cooling plate is considered (*No thermal pad*), the average cell temperature is up to 3K lower in comparison to the experimental data. Without the thermal resistance of the thermal pads, the cooling condition of 30°C is directly connected to the cell bottom made of aluminum. This results in an ideal thermal transfer, which does not correspond to the conditions in the experiment. Therefore, the thermal contact resistance need to be taken into account, as well.

The preliminary results show that only with detailed knowledge of the experiment boundary conditions, which are also considered within the simulation, a validation with high significance is possible. Thus, the validation of the developed cell model was performed with experimental results, measured under the defined boundary condition in BEV environment. Figure 5 shows the results of experiment and simulation for cycling profiles at three different C-rates.

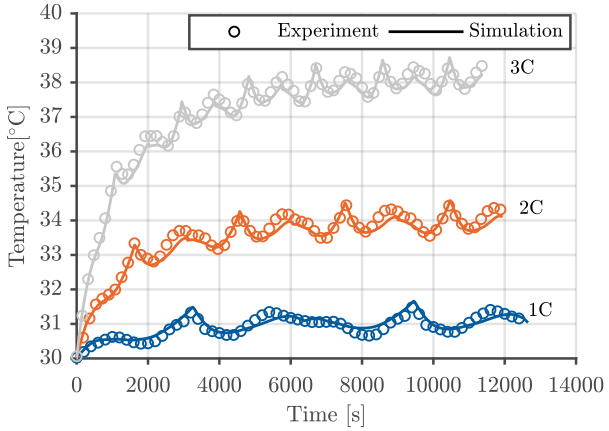

Figure 5: Average cell temperature of experiment and simulation for 25Ah cell cycled with different current profiles under BEV conditions at 30°C.

The model shows very good agreement with the experimental data with an average rms of 0.12K for 1C, 0.19K for 2C and 0.26K for 3C, which are all under the accuracy of the thermocouples of ±0.5K.

All curves of the experiment as well as the simulation show the characteristic shape with rising temperature at the end of charge and discharge step. The characteristic curve shape due to non linear heat generation is implemented in the simulation by the parameters with its SOC and temperature dependency and consideration of SOC-dependent entropic heat. In the case of 1C cycling, the heat generation is manly influenced by the reversible heating, whereas at higher current rates irreversible heating dominates the heat generation, due to the internal resistance. The observed slight deviation at *1C* is probably caused by the used entropic coefficient values. However the discrepancy is rather small and the maximal deviation is 0.27K at 5400s, which is still <1%.

With the MSMD approach and 3D thermal modelling, it is possible to obtain spatially-resolved temperature information as well as electrical behavior. For better validation of the model, the spatial temperature distribution on the cell is experimental validated, using the integrated temperature sensors (see nomenclature in figure 2). In figure 6 are shown the transient temperature evolution at different positions during the experiment and the simulation.

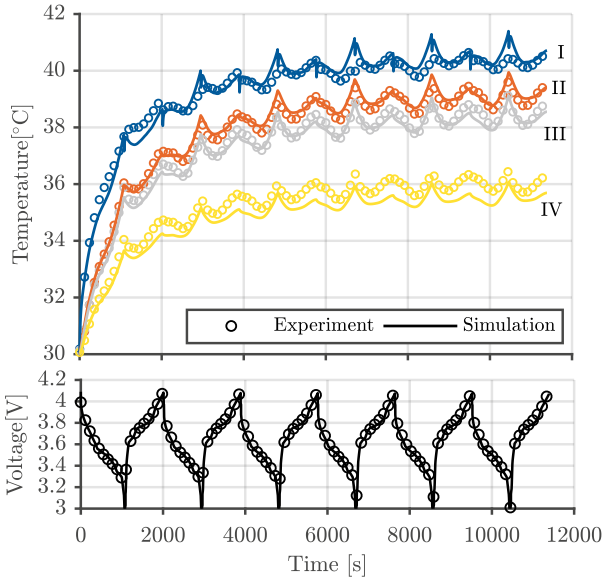

Figure 6: Top: Spatially-resolved cell temperature of experiment and simulation for 25Ah cell cycling with 3C under BEV conditions at 30°C (positions I-IV from figure 2). Bottom: Associated voltage profiles of experiment and simulation.

As it can be seen, the model describes very well the cell voltage behavior during the consecutive charging-discharging. In addition, the model exhibits a good spatially-resolved prediction of the temperature behavior. The terminal temperatures (*I*) are predicted with an average rms of 0.29K with small differences by the first charge cycle and at the end

ISBN 978-1-7281-2078-2

of discharge cycles with advancing time. Very good agreement exists for curve *II* and *III* with no visible difference and average rms values of 0.16K and 0.18K. Curve IV shows a slightly lower temperature with rms of 0.43K. As already shown in figure 4, the contact resistance between the cell housing and the cooling plate has a great impact on simulative results. The underlying material parameters are changed by clamping of the cell on the cooling plate. This affects the thickness as well as the thermal conductivity of the used thermal pad and therefore the results.

Nevertheless, the observed deviation is negligible and the model describes the electrical and thermal cell behavior very well under defined boundary conditions.

5 Conclusion

In this work, an experimental setup was developed on single cell level that takes account of defined boundary conditions, which are reproducible and mimic a BEV-application. An electrical-thermal battery model with detailed 3D thermal model was developed and parametrized. The model takes account of the thermal conditions in BEV-scenario and influences of performed experiments.

The thermal behavior of the studied prismatic cell using different experimental setups were investigated experimentally. The results reveal that boundary conditions such as heat flux in testing equipment, cell bracing and coupling to the cooling system exhibit significant influence on the cell's thermal behavior. The model was validated for average temperature as well as spatially-resolved temperature and electrical behavior. With consideration of the defined boundary conditions of the developed setup the model showed very good agreement to the experimental results.

The performed study points out, that thermal conditions in an experimental setup influence significantly the temperature development. If experimental data is used for validation of a thermal simulation models, all relevant influences and boundary conditions need to be considered in order to describe the cell behavior correctly. Furthermore, the model has to be validated under the same conditions that are later used for simulative-based investigations.

The validated model will be further used to study the thermal cell behavior during dynamic current profiles and varying cooling conditions.

Acknowledgements

The authors wish to acknowledge the extensive discussions with D. Schneider (THI), Dr. M. Hinterberger (Audi AG), Dr. B. Rieger (Audi AG) and R. Reinelt (ANSYS Germany).

Literature

[1] Q. Wang, B. Jiang, B. Li, and Y. Yan, "A critical review of thermal management models and solutions of lithium-ion batteries for the development of pure electric vehicles," Renew. Sustain. Energ. Rev., vol. 64, pp. 106-128, Oct. 2016.

[2] Z. Rao, S. Wang, "A review of power battery thermal energy management," Renew. Sustain. Energy Rev., vol. 15, no. 9, pp. 4554-4571, 2011.

[3] T. M. Bandhauer, S. Garimella, T. F. Fuller, "A critical review of thermal issues in lithium-ion batteries," J. Electrochem. Soc., vol. 158, no. 3, pp. R1-R25, 2011.

[4] S. Erhard, "Multi-dimensional electrochemical-thermal modeling of lithium-ion batteries," Ph.D dissertation, Institute EES, Technical University, Munich, 2017. Accessed on: July. 19, 2019. [Online]. Available: https://mediatum.ub. tum.de/doc/1338266/1338266.pdf

[5] N. A. Samad, J. B. Siegel, A. G. Stefanopoulou, "Parameterization and validation of a distributed coupled electro-thermal model for prismatic cells," Proc. ASME Dyn. Syst. Control Conf., pp. V002T23A006-V002T23A014, 2014.

[6] N. Damay, C. Forgez, M.-P. Bichat, G. Friedrich, "Thermal modeling of large prismatic LiFePO4/graphite battery. Coupled thermal and heat generation models for characterization and simulation," J. Power Sources, vol. 283, pp. 37-45, Jun. 2015.

[7] H. Lundgren et al., "Thermal management of large-format prismatic lithium-Ion battery in PHEV application," J. Power Sources. vol. 163, no. 2, pp. 309-317, Feb. 2015.

[8] D. Bernardi, E. Pawlikowski, and J. Newman, "A general energy balance for battery systems," J. Electrochem. Soc., vol. 132, no. 1, pp. 5–12, 1985.

[9] Shashank Arora, "Selection of thermal management system for modular battery packs of electric vehicles: A review of existing and emerging technologies," J. Power Sources, vol. 400, pp. 621-640, Oct. 2018.

[10] G.H. Kim, K. Smith, K.-J. Lee, S. Santhanagopalan and A. Pesaran, "Multi-domain modeling of lithium-ion batteries encompassing multi-physics in varied length scales," J. Electrochem. Soc., vol. 158, no. 8, pp. 955-969, 2011.

[11] ANSYS Fluent Manual, no. 19.0, ANSYS Inc., Jan. 2018. Accessed on: July. 19, 2019. [Online]. Available: https://ansyshelp.ansys.com

[12] P. Bohn, G. Liebig, L. Komsiyska, G. Wittstock, "Temperature propagation in prismatic lithium-ion-cells after short term thermal stress," J. Power Sources, vol. 313, pp. 30–36, May 2016.

[13] E. Schuster, C. Ziebert, A. Melcher, M. Rohde, and H. J. Seifert, "Thermal behavior and electrochemical heat generation in a commercial 40 Ah lithium ion pouch cell," J. Power Sources, vol. 286, pp. 580-589, Jul. 2015.